CBX 98 - 26
David Asner
Jeff Gronberg
Harry Nelson
May 27, 1998

An Improved dE/dx Calibration for CLEO II/SVX

Abstract

This note outlines a procedure for calibrating dE/dx at the track level in CLEO II/SVX data. This calibration is designed to relate the measured values of pulseheight from the wire hits along the track (DE50) to the fundamental quantity specific ionization (I). While I is expected to be a function of $\beta\gamma$ only it is observed that DE50 is dependent on other quantities. The value of I reconstructed using this technique does not show the same extraneous dependencies as DE50 and we observe 2.1 σ K/π separation at 2.6 GeV/c. No reprocessing is required to use this calibration since the individual hit information is not used. Those wishing to use this calibration but uninterested in the details may want to proceed to Appendix D for instructions on how to apply it to CLEO II/SVX data.

Contents

List of Figures

List of Tables

1 Introduction

1.1 Motivation

In CLEO the specific ionization of a particle is determined from the pulse heights measured on the drift chamber (DR) wires. These pulse heights are combined to form the quantity DE50 which is a central estimate of the ionization. DE50 is a trimmed mean where the lowest 5% and highest 30% of hits are dropped.

We expect the specific ionization of a particle to be solely determined by the particle velocity, β, or equivalently $\beta\gamma$. It is observed in CLEO II/SVX data that the quantity DE50 is not a universal function of $\beta\gamma$ implying that there are systematic effects present.

For instance, we can determine the mean value of DE50 for a sample of kaons and pions kinematically identified in the decay $D^{*+} \to D^o\pi^+$; $D^o \to K^-\pi^+$. Their mean DE50 as a function of $\beta\gamma$ is shown in plot a of Figure 1. The plot shows that pions and kaons with the same $\beta\gamma$ have different values of DE50. The mean DE50's of positive and negative tracks of the same $|\beta\gamma|$ are also different. Since pions and kaons of the same $\beta\gamma$ have different momenta and thus different curvature, we suspected that there was a systematic effect related to curvature.

To test this hypothesis we studied the behavior of DE50 versus curvature for a sample of electrons. The mean DE50 of electrons should be nearly constant, independent of curvature, since in the region of interest they live on the Fermi plateau ($\beta\gamma > 200$). In fact, as can be seen in plot c of Figure 1, the mean DE50 of the electrons depends on both curvature and $\cos\theta$. The changes that depend on curvature, at a given $\cos\theta$, indicate that there is a new systematic effect. The changes that depend on $\cos\theta$ were expected, due to gas gain saturation.

At this point we assumed that whatever effect created the curvature dependence of the electrons was also effecting the pions and kaons in the same way. We determined a set of multiplicative corrections that removed all $\cos\theta$ and curvature dependencies of the electron DE50s. These same corrections were then applied to the pions and kaons. Their DE50 versus $\beta\gamma$ distributions after the correction are shown in plot b of Figure 1. The differences between particle species and the asymmetries between positive and negative tracks were reduced.

Having seen that the behavior of the DE50 variable could be improved we developed a procedure for reconstructing I using as input DE50 and other track level quantities. Since this procedure uses track level quantities it can be applied at the driver level without any need for reprocessing.

1.2 Overview

The relationship between the ionization deposited in a cell and the pulse height read out of the ADC has a number of complications:

- The ionization deposited in the cell must drift to the readout wire. The fraction of the ionization that reaches the wire is a function of the drift distance and the entrance angle to the cell.
- The ionization that reaches the wire is amplified by the gas gain. The gas gain can vary from run to run due to changes in atmospheric pressure and DR voltages. Also as the charge per unit length along the wire increases the gas gain saturates and reduces the total charge read out of the ADC.

We have no access to information about individual hits since we are working at the track level. However, we expect that these hit level effects will correlate with certain track level quantities.

- For tracks with zero impact parameter there is a fixed relationship between curvature, radius of a cell and entrance angle to that cell. Tracks with a particular curvature will therefore sample a consistent set of entrance angles.
- The gas gain saturation should be a function of charge per unit length along the wire, $f(Q/\Delta Z)$. The quantity $Q/\Delta Z$ is proportional to $\mathrm{DE50}/\cos\theta$, which is the ionization along the track projected onto the z axis.

Given these relationships our calibration procedure will be as follows:

- The mean DE50 for electrons is a function of $\cos\theta$ and curvature although electrons above 100 MeV/c are expected to have a uniform ionization. Therefore we will construct a function of $\cos\theta$, curvature, run number and bunch number that transforms DE50 to a new variable $\mathrm{DE50_{elec}}$. The function is chosen so that the mean value of $\mathrm{DE50_{elec}}$ is a constant for electrons.
- We expect that particles with values of $\mathrm{DE50_{elec}}$ different from electrons will still exhibit a $\cos\theta$ dependence from gas gain saturation. We will use protons, which have $\mathrm{DE50_{elec}}$ larger than the electrons, and pions and muons, which have $\mathrm{DE50_{elec}}$ smaller than the electrons to parameterize this effect. We will then construct a variable I from $\mathrm{DE50_{elec}}$ and $\cos\theta$ where the mean value of I shows no $\cos\theta$ dependence.
- We will then parameterize the mean and width of the I distributions and use those parameterizations to construct the SGXXDI variables, which give the number of standard deviations a track differs from the XX hypothesis.

We have motivated the need for an improved calibration in this section and given an overview of the calibration procedure. In the next section we detail each step in the calibration procedure. The details and difficulties in obtaining the calibration data samples are described in the appendices.

2 Calibration Procedure

2.1 Introduction

In the standard CLEO dE/dx calibration it is noted that ionization from electrons and ionization from pions do not seem to follow the same drift function. The current calibration therefore uses two sets of constants to describe the drift function of the wires, despite the fact that there is, in reality, only one drift function. There is one set of constants for hadrons and one for electrons:

1. electron constants - calculated with bhabhas
2. hadron constants - calculated with π's from K_{s}^{o}

Each set of constants can be used to calculate a value of DE50 for a track and each gives a different value of DE50.

This effect is apparently due to an error in the calculation of entrance angle for tracks that have large impact parameter, such as π's from K_{s}^{o}. Once this problem was corrected it was observed that pions and electrons behaved essentially the same, as expected. Since the hadron constants are calculated using tracks with large impact parameters we expect that the DE50's calculated using hadron constants will be miscalibrated. The calibration described in this note corrects the DE50's calculated with hadron constants using information available at the track level, as described previously. Work is currently in progress to correct the individual hits but this will require reprocessing before it can become available. This track level calibration can be directly applied to the hadron skims without any reprocessing.

2.2 Electron Calibration

We have skimmed a sample of $\gamma\gamma \rightarrow e^{+}e^{-}$ events (see Appendix C.2) which provides us with electrons from 100 MeV/c to 5 GeV/c. This corresponds to values of $\beta\gamma$ from 200 to 10,000. This region of $\beta\gamma$ is called the Fermi plateau, where specific ionization is nearly a constant, with only an order 3% drop in ionization as $\beta\gamma$ approaches 200. After correcting for the small running in $\beta\gamma$ we have a sample of particles of uniform ionization.

We use a sample of electrons whose value of DE50 is calculated with *hadron* constants to probe the behavior of the hadron constants. We note that they exhibit dependence on both $\cos\theta$ and curvature as seen in plot c of Figure 1. Our procedure will be to parameterize the dependence of DE50 on $\cos\theta$, curvature, run number and bunch number and then remove it, creating a new variable, $\mathrm{DE50_{elec}}$, where $\mathrm{DE50_{elec}}$ for electrons is chosen to be 1.15 in units that are arbitrary, but nearly equivalent to DE50.

In plot a of Figure 2 we see mean DE50 for electrons plotted versus run number. Each point is a sum over several runs (~ 10) so that each point contains at least 1200 electrons. The points are well behaved except for a region in the 4sL and 4sM where there was a change in the calibration procedure. The old procedure was reinstated for 4sN. The odd scattering of points in the 4sL is not understood.

In plot b of Figure 2 we see the mean DE50 for electrons plotted versus bunch number for the 4sM data. There is a nearly linear relationship between the charge collected and the bunch number of the interaction. This is because the shaped pulse is latched into the ADC on it's falling edge, therefore tracks from later bunches get latched into the ADC when they are closer to their peak.

Once the run dependent variations are removed we examine the behavior of the electrons as a function of $\cos\theta$ and curvature. The $\gamma\gamma \to e^+e^-$ sample illuminates the entire region of interest in these variables. We bin the tracks in 1600 bins, 40 in curvature and 40 in $\cos\theta$. The behavior of the electron's mean DE50 as a function of curvature can be seen in plot c of Figure 2. For large curvature (low momentum) no dependence is seen. However, for curvatures < 0.36 (> 600 Mev/c) there is a nearly linear relationship between curvature and mean DE50. The slope of this line is different for positive and negative tracks by 50%.

The behavior of the electron's mean DE50 as a function of $\cos\theta$ can be seen in plot d of Figure 2. We expect to see gas gain saturation effects in this variable. As $\cos\theta \to 0$, charge per unit length becomes large, therefore, mean DE50 should decrease. This is exactly the behavior we see. There is a discontinuity in the distribution around $|\cos\theta| = 0.7$ that is not understood. This is the boundary between barrel and endcap tracks but in principle we do not expect any dependence of the mean DE50 on that.

We parameterize the mean DE50 for electrons with 40 constants, one for each bin in $\cos\theta$ and two smooth curves that are functions of curvature (κ), one for each charge. The two curves and the 40 constants are shown in plots b and c of Figure 2. These parameters give us a set of scale factors that can be used to construct the quantity $\mathrm{DE50}_{\mathrm{elec}}$.

$$\begin{array}{ll} \mathrm{scale} = \mathrm{const}(\theta) & \mathrm{abs}(\kappa) > \mathrm{offset} \\ \mathrm{scale} = \mathrm{const}(\theta) + \mathrm{slope} * (\mathrm{abs}(\kappa) - \mathrm{offset}) & \mathrm{abs}(\kappa) < \mathrm{offset} \end{array} \tag{1}$$

We then construct $\mathrm{DE50}_{\mathrm{elec}}$ using the formula:

$$\mathrm{DE50}_{\mathrm{elec}} = \left(\frac{1.15}{\mathrm{scale}}\right) \mathrm{DE50} \tag{2}$$

Having developed a correction using the electrons we now examine the effect of this correction on other particles. We use a variety of data samples, described in Appendices A, B and C, to probe a large range of $\beta\gamma$. The physics processes and the corresponding $\beta\gamma$ coverages are:

Sample:	$\beta\gamma$ region:
protons	0.2 - 1.0
$e^+e^- \to \pi^+\pi^-\pi^+\pi^-$	1.0 - 10.0
$e^+e^- \to \mu^+\mu^-\gamma$	10.0 - 50.0

We determine the mean DE50 for these particles after binning them in $\cos\theta$ and curvature. The results are shown in plot a of Figure 3. While we do not have a prediction for what the value of DE50 should be at a particular $\beta\gamma$, we know that at a fixed $\beta\gamma$ there should be no $\cos\theta$ dependence. Again, just as in the electrons, we do see a $\cos\theta$ dependence in these points. Also at $\beta\gamma = 50$, which correspond to 5 Gev/c muons, there is a difference between positive and negative tracks. Plot b in Figure 3 shows the same data after the electron correction has been applied. The $\cos\theta$ dependence and the asymmetry between positive and negative tracks is greatly reduced.

2.3 Gas Gain Non-linearity Calibration

After the deposited ionization has drifted to the wire it undergoes an avalanche in the high electric field region around the wire which results in amplification of the signal. As the density of ionization increases there is a tendency of the charges to partially cancel the electric field resulting in a loss of gain. The gas gain should thus be a function of the charge density along the wire. For a given track the charge density is given by the ionization (I) of the track projected onto the z axis.

$$\frac{\Delta Q}{\Delta Z} = \frac{\mathrm{I}}{\cos\theta + \delta_g} \tag{3}$$

The parameter δ_g models the longitudinal spreading of the avalanche and prevents infinite charge density. It should be noted that this quantity is independent of how the track intersects a cell.

We expect that for a constant ionization the measured DE50 will decrease as $\cos\theta$ goes to zero since this corresponds to increasing charge density. We choose to parameterize the relationship between actual ionization (I) and measured ionization (D) using this formula:

$$I = \mathrm{D}\,\frac{\beta + \alpha\left(\frac{\mathrm{D}}{\cos\theta+\delta_g}\right)}{1 + \gamma\left(\frac{\mathrm{D}}{\cos\theta+\delta_g}\right)} \tag{4}$$

Where D is a hypothetical measurement where all effects other than gas gain saturation have been removed, and β is arbitrary; we choose it to be 1. The function is shown in plot a in Figure 4. For small values of I there is a linear relationship between I and D independent of $\cos\theta$. As I increases there is an increasing dependence on $\cos\theta$ which causes the curves to diverge. This would result in the most normal tracks ($\cos\theta = 0$) having the smallest measured ionization.

In the real detector, however, we do not measure D but instead measure $\mathrm{DE50_{elec}}$. This means that for the value of ionization that corresponds to the electrons, $\mathrm{DE50_{elec}}$ has a single value independent of $\cos\theta$, as shown in plot b of Figure 4. This has the effect of moving the curves together but undercorrects particles with ionization larger than the electrons and overcorrects particles with ionization smaller than the electrons. When we look at the

Table 1: Parameters of Gas Gain Nonlinearity Calibration. β is chosen to be 1.0.

α	0.0336 ± 0.0017
β	1.000
γ	-0.01913 ± 0.0014
δ_g	0.1021 ± 0.0040
cp	1.1025 ± 0.0038

behavior of the pions, muons and protons this is exactly the behavior we see. In Figure 5 we see in plot a that for protons the most normal points have the smallest values of measured ionization. Plot b is a blow up of the region around minimum ionization. In that region the most normal points have the largest value of measured ionization.

In order to determine the parameters which describe the gas gain saturation we perform a fit assuming that tracks with the same $\beta\gamma$ but different $\cos\theta$ have the same ionization. First we must convert $\mathrm{DE50_{elec}}$ to D. To do this we choose I for electrons to be 1.15. Then for any set of parameters; α, β, γ and δ_g we can compute the value of D for electrons as a function of $\cos\theta$ which we call $D_e(\cos\theta; \alpha, \beta, \gamma, \delta_g)$. We allow the cross-over point (cp), where $\mathrm{DE50_{elec}}$ is the same for all values of $\cos\theta$, to vary. Then we can rewrite the parameterization in term of $\mathrm{DE50_{elec}}$:

$$I = \frac{D_e(\cos\theta; \alpha, \beta, \gamma, \delta_g)}{\mathrm{cp}} \mathrm{DE50_{elec}} \frac{\beta + \alpha \left(\frac{D_e(\cos\theta;\alpha,\beta,\gamma,\delta_g)}{\mathrm{cp}} \frac{\mathrm{DE50_{elec}}}{\cos\theta+\delta_g} \right)}{1 + \gamma \left(\frac{D_e(\cos\theta;\alpha,\beta,\gamma,\delta_g)}{\mathrm{cp}} \frac{\mathrm{DE50_{elec}}}{\cos\theta+\delta_g} \right)} \tag{5}$$

A fit to the proton, pion and muon samples yield the paremeters in table 1. In figure 6 we show the $\cos\theta$ dependence of the points before and after the saturation correction for protons with large ionization in plot a and for pions around minimum ionization in plot b. The value of I computed using these parameters for protons and pions around minimum ionization is shown in plots c and d of Figure 5. At this point we believe that we have removed all dependencies of the measured ionization on $\cos\theta$ and curvature.

2.4 Residual non-linearity correction

After the previous corrections it is observed that the "$1/\beta^2$" region does not actually run as $1/\beta^2$. This is due to the residual non-linearity between actual and measured ionization. We impose a transformation that improves the behavior of this region of the form:

$$I = 2.862 \times I^{0.3860} - 1.862 \tag{6}$$

2.5 Empirical Model of I vs $\beta\gamma$

The previous corrections have removed the dependence of I on $\cos\theta$ and curvature. We can now parameterize the mean value of I ($\overline{I}$) as a function of $\beta\gamma$. We fit three regions in $\beta\gamma$ to a power law + third order polynomial.

$$\overline{I} = A\,(\beta\gamma)^n + P_o + P_1\,(\beta\gamma) + P_2\,(\beta\gamma)^2 + P_3\,(\beta\gamma)^3 \tag{7}$$

Figure 7 shows the fit to the data and table 2 lists the fit parameters. The region of $|\beta\gamma| > 200$ is described by a single parameter, $\overline{I} = 1.2132$.

Table 2: Parameters for Power Law + 3rd Order Polynomial fit to $\overline{I}$ vs $\beta\gamma$; $\overline{I} = A\,(\beta\gamma)^n + P_0 + P_1\,(\beta\gamma) + P_2\,(\beta\gamma)^2 + P_3\,(\beta\gamma)^3$.

$\beta\gamma$ region	A	n	P_0	P_1	P_2	P_3
0.0-1.0	0.10941	-3.00822	4.50657	-6.17805	3.93076	-0.87888
1.0-8.0	0.86559	-1.62923	0.54515	0.08684	-8.10047×10^{-3}	3.27413×10^{-4}
8.0-100.0	-0.88992	-0.01789	1.67977	0.01397	-2.68168×10^{-4}	1.85736×10^{-6}
> 200.0	$\overline{I} = 1.2132$					

2.6 Running in number of hits

Each track can have from 10-50 wire hits included in its measurement of the ionization. After the curvature and gas gain calibrations a small dependence of $\overline{I}$ on NHITDI is observed, as shown in plot a of Figure 8. We divide the data into four regions; $|\cos\theta| > .7$,$|\cos\theta| < .7$ and NHITDI > 37, NHITDI < 37 and remove this effect with four separate linear parameterizations. The points after this correction are shown in plot b of Figure 8.

NHITDI	$\lvert\cos\theta\rvert$	slope $\times 10^{-4}$	intercept $\times 10^{-2}$
< 37	> 0.7	-4.82 ± 1.84	1.24 ± 0.58
> 37	> 0.7	2.53 ± 2.78	-1.23 ± 1.16
< 37	< 0.7	19.2 ± 15.2	-6.17 ± 4.86
> 37	< 0.7	-8.76 ± 0.99	3.77 ± 0.43

2.7 Empirical Determination of σ_I

The track level quantity I can be thought of as the total charge (Q) deposited by the track divided by the total path length of the track. The error on Q should be proprotional to $\sqrt{Q}$ and therefore the error on I should be given by

$$\sigma_I \propto \frac{\sqrt{Q}}{\text{path length}} = \frac{\sqrt{I} \times \text{path length}}{\text{path length}} = \frac{\sqrt{I}}{\sqrt{\text{path length}}} \tag{8}$$

$$\text{path length} \propto \text{NHITDI}/\sin\theta \tag{9}$$

where NHITDI is the number of dE/dx hits used for that track. Given that we expect the σ_I to behave this way we choose to parameterize the behavior in terms of three functions:

$$\sigma_I = \frac{f\left(I^{1/2}\right)}{g\left(\text{NHITDI}^{1/2}\right) h\left(1/\sin\theta^{1/2}\right)} \tag{10}$$

We divide the data into bins of NHITDI, $\sin\theta$ and $\beta\gamma$. For each bin we determine the mean value of I and the width of the I distribution. The measured width of the distribution must be corrected for the $\beta\gamma$ running of I over the width of the bin. We use the parameterization of $\overline{I}$ to remove this effect. The width for each point is shown in plot a of Figure 9. The next three plots show the functional form of $f\left(I^{1/2}\right)$, $g\left(\text{NHITDI}^{1/2}\right)$ and $h\left(1/\sin\theta^{1/2}\right)$ where the effect of the other two functions have been removed. The parameterizations of the functions are given below.

$$\begin{array}{ll} f\left(I^{1/2}\right) = 0.45 + 0.087(I^{1/2} - 1.1) & I^{1/2} < 1.1 \\ f\left(I^{1/2}\right) = 0.45 + 0.52(I^{1/2} - 1.1) - 0.23(I^{1/2} - 1.1)^2 + 0.515(I^{1/2} - 1.1)^3 & I^{1/2} > 1.1 \end{array} \tag{11}$$

$$g\left(\text{NHITDI}^{1/2}\right) = \text{NHITDI}^{1/2} - 1.306 \tag{12}$$

$$h\left(1/\sin\theta^{1/2}\right) = 1/\sin\theta^{1/2} + 0.261 \tag{13}$$

2.8 Generation of SGXXDI variables

Now that we have a parameterization of the mean and expected width of the I distribution constructing the SGXXDI variables is simple. For a particle hypothesis (XX $= e$, μ, π, K, proton) the expected value of $\beta\gamma$ is equal to the momentum of the track divided by the particle mass (P/M_{XX}). Using this value of $\beta\gamma$ we find the expected value of $\overline{I}$. Using that value of $\overline{I}$ along with the number of hits on the track and it's value of $\sin\theta$ we can determine σ_I. Then the value of SGXXDI is given by:

$$\text{SGXXDI} = \frac{I - \overline{I}}{\sigma_I} \tag{14}$$

The SGXXDI variables constructed in this manner are shown in Figures 10 through 14 for the various data sets and calibration samples, they are all unit gaussians centered at zero.

2.9 π/K Separation

For a track with a particular momentum we can compute $\beta\gamma$ for the pion and kaon hypotheses. Using those values we can compute the difference in the mean value of I for pions and kaons using our parameterization of $\overline{I}$. Then, using a measured spectrum of NHITDI and $\sin\theta$ for real pions and kaons from D^o decay the expected width can be used to predict the separation between pions and kaons at that momentum. In order to verify that the expected width is the same as the actual width we construct the appropriate SGXXDI for these tracks and measure the width of the distribution (σ_{Pull}), we scale the expected width by this factor. The formula for the K/π separation is given by:

$$\sigma_{(\pi \text{ fakes K})} = \frac{|\overline{I}(\text{pion}) - \overline{I}(\text{kaon})|}{\sigma_I(\text{pion})\sigma_{\mathrm{Pull}}(\text{pion})} \tag{15}$$

similarly the π/K separation is given by replacing the pion width with the kaon width:

$$\sigma_{(\text{K fakes } \pi)} = \frac{|\overline{I}(\text{pion}) - \overline{I}(\text{kaon})|}{\sigma_I(\text{kaon})\sigma_{\mathrm{Pull}}(\text{kaon})} \tag{16}$$

In Figure 15 there are three plots which show the K/π separation calculation. Plot a is the difference in $\overline{I}$ for pions and kaons as a function of momentum. Calibration points are black, actual pions and kaons from D^o decay are shown in red. Plot b shows the mean fitted value of predicted width for the actual pions from D^o decay. Plot c is the fitted width of the pull distribution for those points. In Figure 16 the results of the K/π separation calculation are shown. In the region of the $B \to K/\pi$ decay we predict 2.1σ separation between kaons and pions.

2.10 Conclusion

We have observed that the variable DE50 is not a universal function of $\beta\gamma$ and is thus not a systematic free estimator of the ionization of a track. We have created a procedure for constructing a new variable I, which is a function of the track parameters and the value of DE50. This variable is a more universal function of $\beta\gamma$. We construct the SGXXDI variables after parameterizing the mean and width of the I distribution. The SGXXDI variables thus constructed are unit gaussians centered at zero. We observe 2.1 σ K/π separation in the CLEO II/SVX data using these variables.

A Summary of CLEO II/SVX Datasets

The current CLEO II/SVX integrated luminosity exceeds $6fb^{-1}$. At the time of writing this CBX, data sets 4sJ-4sN have been pass2'ed, The 4sH, 4sP and 4sQ data sets await processing and the current data set is the 4sR.

Dataset	Usable Luminousity (pb^{-1})	# of tapes Full Roar + Muons
4sH	153.0	N/A
4sJ	677.0	65+1
4sK	595.0	69+1
4sL	1080.6	93+3
4sM	531.8	48+N/A
4sN	714.3	74+1
4sP	1103.6	N/A+N/A
4sQ	560.0	N/A+N/A

Table 3: Summary of Luminousity and DLT tapes by dataset. N/A indicates data unavailable at time of calibration

The skims required for this analysis come in three varieties, Full Roar data and Full Roar Muon skim on DLT and hadron skims on disk. We run on the Full Roar data and the hadron skims to generate 5 additional skims. Table 3 contains a summary of luminousity and DLT tapes for each dataset.

1. Full Roar data on DLT
   (a) $\gamma\gamma \to 2e$
   (b) $e^+e^- \to \mu^+\mu^-\gamma$
   (c) $\gamma\gamma \to 4\pi$
2. Full Roar Muons on DLT
3. Hadron skims on disk.
   (a) K and π from $D^{*+} \to D^o\pi_s^+, D^o \to K^-\pi^+$
   (b) Protons

B dE/dx Calibration Skims

All events samples required for the dE/dx calibration of 4sJ-N datasets are available on DLT. These tapes, named 4sX_DEDX_SKIM, can be requested in the Batch Queues. The cross section skimmed and the cross section used in the calibration for each skim and each dataset is summarized in table 4. The files on each tape are in .rp or .rp.gz format with block size 32400. The contents of each tape is listed below

4sJ_DEDX_SKIM: 197 files

1. 65 files $\gamma\gamma \rightarrow 2e$ from 4sJ_FR01-4sJ_FR65
2. 65 $\gamma\gamma \rightarrow 4\pi$ from 4sJ_FR01-4sJ_FR65
3. 65 $e^+e^- \rightarrow \mu^+\mu^-\gamma$ from 4sJ_FR01-4sJ_FR65
4. 2 proton files, from Hadron skims. These two files are gzipped.

4sK_DEDX_SKIM: 209 files

1. 69 files $\gamma\gamma \rightarrow 2e$ from 4sK_FR01-4sK_FR69
2. 69 $\gamma\gamma \rightarrow 4\pi$ from 4sK_FR01-4sK_FR69
3. 69 $e^+e^- \rightarrow \mu^+\mu^-\gamma$ from 4sK_FR01-4sK_FR69
4. 2 proton files, from Hadron skims. These two files are gzipped.

4sL_DEDX_SKIM: 197 files

1. 8 files $\gamma\gamma \rightarrow 2e$ from 4sL_FR01-4sL_FR93
   - 1 huge file containing all 4sL_FR01-4sL_FR93 except tapes 9,26,48,59,91,92,93
   - 4sL_FR09
   - 4sL_FR26
   - 4sL_FR48
   - 4sL_FR59
   - 4sL_FR91
   - 4sL_FR92
   - 4sL_FR93
2. 93 $\gamma\gamma \rightarrow 4\pi$ from 4sL_FR01-4sL_FR93
3. 93 $e^+e^- \rightarrow \mu^+\mu^-\gamma$ from 4sL_FR01-4sL_FR93
4. 3 proton files, from Hadron skims. These three files are gzipped.

4sM_DEDX_SKIM: 146 files

1. 48 files $\gamma\gamma \rightarrow 2e$ from 4sM_FR01-4sM_FR48
2. 48 $e^+e^- \rightarrow \mu^+\mu^-\gamma$ from 4sM_FR01-4sM_FR48

3. 48 $\gamma\gamma \to 4\pi$ from 4sM_FR01-4sM_FR48

4. 2 proton file, select run # 87049-88467 from Hadron skims

4sN_DEDX_SKIM: 224 files

1. 74 files $\gamma\gamma \to 2e$ from 4sN_FR01-4sN_FR74

2. 74 $\gamma\gamma \to 4\pi$ from 4sN_FR01-4sN_FR74

3. 74 $e^+e^- \to \mu^+\mu^-\gamma$ from 4sN_FR01-4sK_FR74

4. 2 proton files, from Hadron skims. These two files are gzipped.

DSTAR_SKIMS_ASNER: 16 files, $D^{*+} \to D^o\pi_s^+, D^o \to K^-\pi^+$, The first 11 files are a loose skim and the last 5 files are a tighter skim of the same data.

- loose skim
  1. 2 files 4sJ, gzipped
  2. 2 files 4sK, gzipped
  3. 3 files 4sL, gzipped
  4. 2 files 4sM, gzipped
  5. 2 files 4sN, gzipped
- tight skim
  1. 1 file 4sJ
  2. 1 file 4sK
  3. 1 file 4sL
  4. 1 file 4sM
  5. 1 file 4sN

C Selection Criteria for Event Sample

C.1 Good Track Criteria

1. NHITCD ≥ 15

2. KINCD $= 0$

3. Not a DUET dredge seed

4. Not a Z-Escape

5. Trackman Approved

Data Set	Skim	Number of Events Skimmed	Effective Cross Section Skimmed (pB)	Number of Tracks Used in Calibration
4sJ 592 pb^{-1}	$\gamma\gamma \to 2e$	152623	264.5	151672
	$\gamma\gamma \to 4\pi$	22821	38.5	31652
	$e^+e^- \to \mu^+\mu^-$	185628	313.6	255570
	$e^+e^- \to \mu^+\mu^-\gamma$	65815	111.2	25091
	Kaons	21788	38.4	836
	Protons	231818	408.1	51989
4sK 632 pb^{-1}	$\gamma\gamma \to 2e$	184248	291.5	193658
	$\gamma\gamma \to 4\pi$	24608	38.9	31876
	$e^+e^- \to \mu^+\mu^-$	194777	308.2	261793
	$e^+e^- \to \mu^+\mu^-\gamma$	73225	115.9	28962
	Kaons	21498	36.6	1126
	Protons	181378	308.5	83665
4sL 1.14 fb^{-1}	$\gamma\gamma \to 2e$	316748	277.8	310347
	$\gamma\gamma \to 4\pi$	43122	37.8	64866
	$e^+e^- \to \mu^+\mu^-$	476785	418.2	633628
	$e^+e^- \to \mu^+\mu^-\gamma$	135209	118.6	51806
	Kaons	37809	38.0	1615
	Protons	287726	289.2	137726
4sM 592 pb^{-1}	$\gamma\gamma \to 2e$	142773	241.2	142103
	$\gamma\gamma \to 4\pi$	22988	38.8	33557
	$e^+e^- \to \mu^+\mu^-$	N/A	N/A	N/A
	$e^+e^- \to \mu^+\mu^-\gamma$	70370	118.9	28144
	Kaons	24225	41.0	1089
	Protons	160358	271.3	79710
4sN 768 pb^{-1}	$\gamma\gamma \to 2e$	197934	257.7	198158
	$\gamma\gamma \to 4\pi$	31708	41.3	45721
	$e^+e^- \to \mu^+\mu^-$	277942	361.9	396279
	$e^+e^- \to \mu^+\mu^-\gamma$	92095	119.9	36377
	Kaons	30658	40.2	1282
	Protons	223008	292.3	111010

Table 4: Summary of cross sections of dE/dx skims. Uncertainty in luminosity and effective cross section is $\sim 1\%$. Detector effects and varying run conditions are likely to alter the effective cross sections significantly.

C.2 $\gamma\gamma \to 2e$

C.2.1 Skim Criteria

- KLASGL ≥ 4
- Only 2 oppositely charge tracks or only 2 oppositely charged tracks passing trackman
- $P_t < 200$ MeV
- E/p > 0.85 for both tracks
- $0.95 < \beta_{tf} < 1.15$ for both tracks

C.2.2 Additional Quality Cuts for Electron Calibration

- Likelihood of e^+e^- beamspot vertex $> 5\%$
- E/p > 0.90 for both tracks
- χ^2 of kalman track fit < 1.5
- DEDX hits > 10

C.3 $\gamma\gamma \to 4\pi$

C.3.1 Skim Criteria

- KLASGL ≥ 4
- Only 4 tracks with zero net charge or only 4 tracks passing trackman with zero net charge
- $P_t < 200$ MeV
- Require $\gamma\gamma \to 2\rho$, $|M_\rho - M_{\pi\pi}| < 150$ MeV

C.3.2 Additional Quality Cuts for Nonlinearity Calibration

- χ^2 of kalman track fit < 1.5
- DEDX hits > 10
- Require good track
- DPTHMU $= 0.0$
- $|SGPITF| < 2.0$

- $|SGPRTF| > 3.0$ or $P_\pi > 1.0$ GeV
- Require a shower match and E/p < 0.80
- $\beta\gamma > 1.5$

C.4 $e^+e^- \to \mu^+\mu^-$

C.4.1 Skim Criteria

CLEO mu skim criteria

C.4.2 Additional Quality Cuts for Nonlinearity Calibration

- One unmatched shower, E > 0.2 GeV
- One track with DPTHMU > 7.0
- KLASGL $\neq 4$
- χ^2 of kalman track fit < 1.5
- DEDX hits > 10
- Require good track
- MUQUAL $= 0.0$
- DPTHMU > 5.0
- E9/E25 > 0.95
- E/p < 0.2

C.5 $e^+e^- \to \mu^+\mu^-\gamma$

- Require 2 good tracks
- 1 track with DPTHMU > 3.0
- $\delta\phi > 0.2$ radians
- One track $1.0 < p < 4.0$ GeV

C.5.1 Additional Quality Cuts for Nonlinearity Calibration

- One unmatched shower, E > 0.2 GeV
- One track with DPTHMU > 7.0
- KLASGL = 4
- χ^2 of kalman track fit < 1.5
- DEDX hits > 10
- Require good track
- MUQUAL = 0.0
- DPTHMU > 3.0
- E9/E25 > 0.95
- E/p < 0.2

C.6 Protons

C.6.1 Skim Criteria

- $1.5 < \beta^{-1} < 4.0$
- TFIDQL $\neq$ 0 and #TF tubes = 2
- TFMASS > 0.8 MeV

C.6.2 Additional Quality Cuts for Nonlinearity Calibration

- χ^2 of kalman track fit < 1.5
- DEDX hits > 10
- Require good track
- $|SGPRTF| < 2.0$
- DPTHMU = 0.0

C.7 K and π from $D^{*+} \rightarrow D^o \pi_s^+, D^o \rightarrow K^- \pi^+$

C.7.1 Skim Criteria

- KLASGL = 10
- $P_k, P_\pi > 100$ MeV, $P_{\pi_s} > 50$MeV
- K and π oppositely charged
- $|M_{K\pi} - M_D| < 210$ MeV
- $|M_{K\pi\pi_s} - M_{K\pi} - M_\pi - 5.85 MeV| < 7.5$ MeV
- $P_{D^*} > 1.9$ GeV

C.7.2 Additional Quality Cuts for Nonlinearity Calibration

- Require K,π and π_s are good tracks
- $\pi_s \geq 2$ SVX hits/view
- $|M_{K\pi} - M_D| < 14$ MeV
- $|M_{K\pi\pi_s} - M_{K\pi} - M_\pi - 5.85 MeV| < 500$ keV
- $P_{D^*} > 2.0$ GeV
- Likelihood of D^o vertex $> 1\%$
- Likelihood of π_s refit through primary vertex $> 0.1\%$

D Applying the corrections at the DRIVER level

In order to apply these corrections the user should call TLDIFX after GETCD in their ANAL3 routine. The subroutine call will overwrite the variables de50di,resdi and the five sgxxdi variables for each track in the event that has IQALDI$\neq$0.

Some important caveats about this calibration. This fix is only valid for tracks that come from the origin. The relationship between entrance angle and curvature breaks down when the particles have a non-zero impact parameter. No problems have been seen in continuum D^o's or $D^\pm$'s but for tracks from K_s^o and Λ there should be a definite widening of the sgxxdi distributions. It is expected that improvements in the hit level calibration procedure will eventually remove this effect.

The function used to model the gas gain saturation is not valid for very large values of measured pulse height. In 0.05% of tracks in hadronic events the dedx correction fails. This should be a problem only for kaons below 200 Mev/c and protons below 400 MeV/c. When the correction fails the origional sgxxdi values are left unchanged.

References

[1] R.M. Sternheimer et al, "The Density Effect for the Ionization Loss of Charge Particles in Various Substances", Atomic Data & Nuclear Data Tables (30), 261-271 (1984)

[2] W. W. M. Allison & J. H. Cobb, "Relative Charged Particle Identification by Energy Loss", Ann. Rev. Nucl. Part. Sci. (30), 253-298 (1980)

[3] A. H. Walenta et al, "Measurement of the Ionizatioin Loss in the Relativistic Rise for Noble and Molecular Gases", Nuclear Instruments and Methods (161), 45-58 (1979)

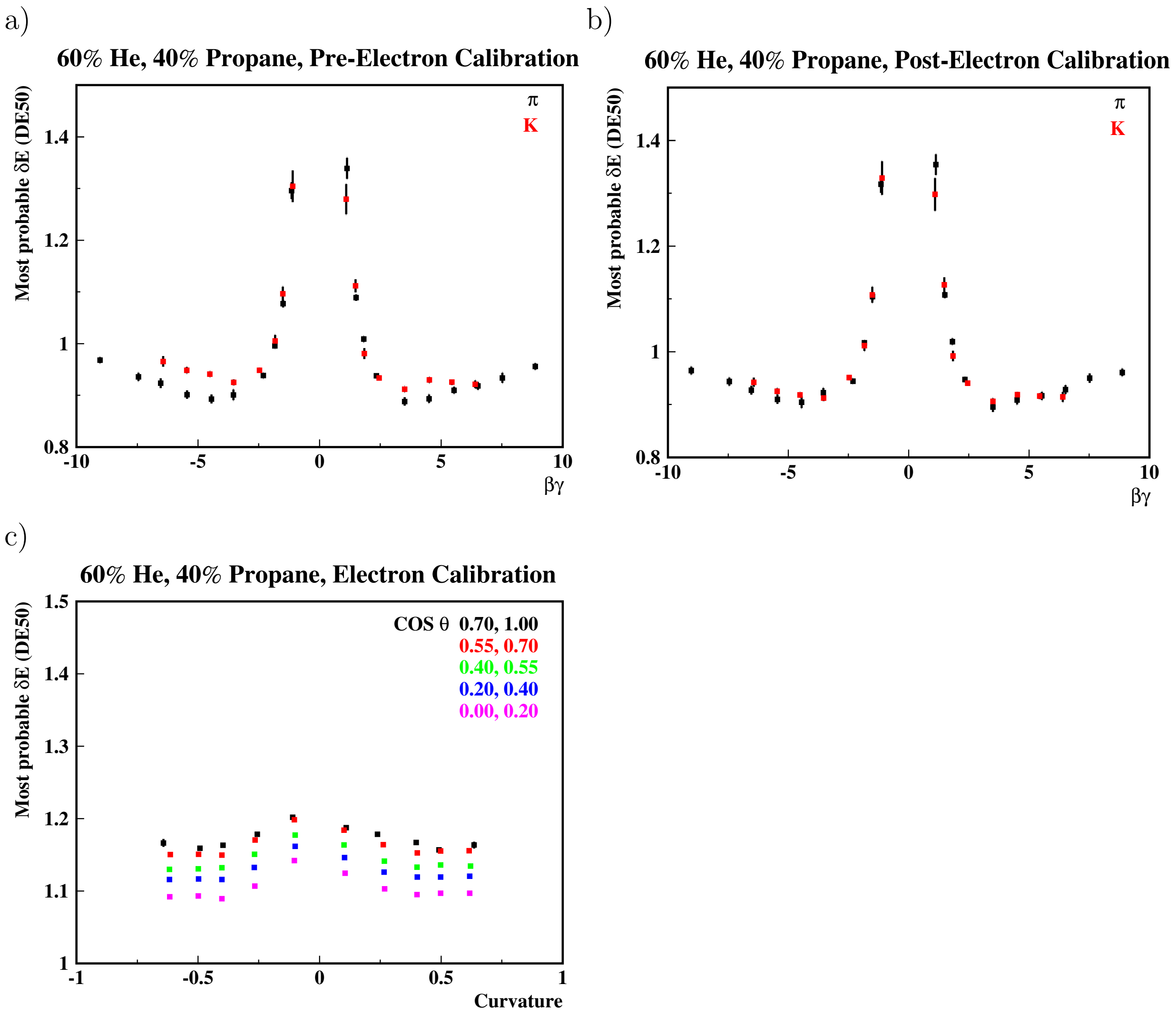

Figure 1: The most probable DE50 for π and K from $D^{*+} \rightarrow D^o\pi_s^+, D^o \rightarrow K^-\pi^+$. Plot a shows the values after only run by run normalization. Plot b shows the values after the electron correction. The dependence of the most probable DE50 for electrons on $\cos\theta$ and curvature is shown in plot c.

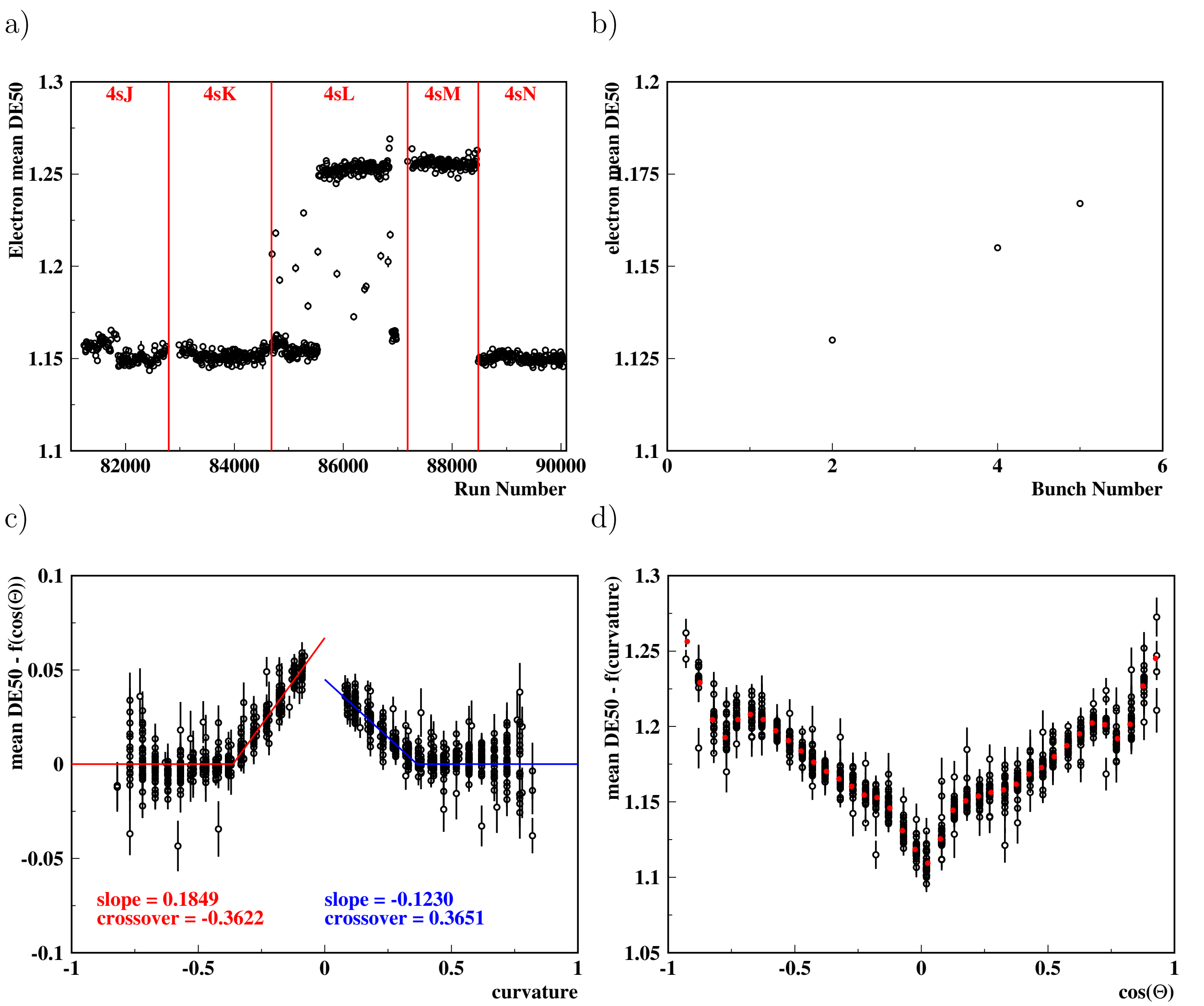

Figure 2: Each plot shows the mean DE50 for electrons versus a variable after the dependence on the other three variables have been removed. Plot a shows the dependence on run number. Plot b shows the dependence on bunch number. Plot c shows the curvature dependence and plot d shows the $\cos\theta$ dependence.

a) b)

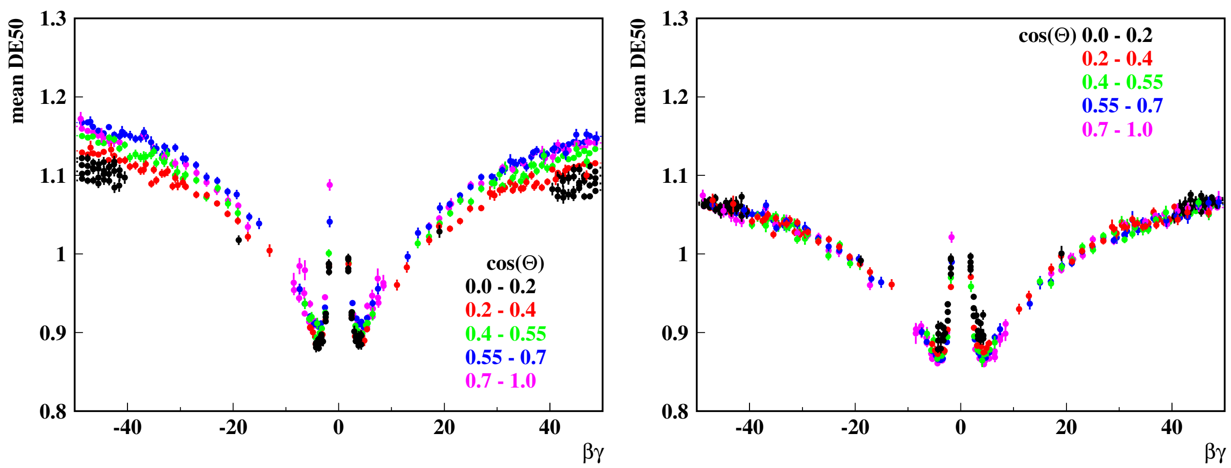

Figure 3: The $\cos\theta$ dependence of mean DE50 for pions and muons for $\beta\gamma$ from 1 to 50. Plot a shows the values after only run by run normalization. Plot b shows the mean value of $\mathrm{DE50}_{\mathrm{elec}}$ for the same tracks.

a) b)

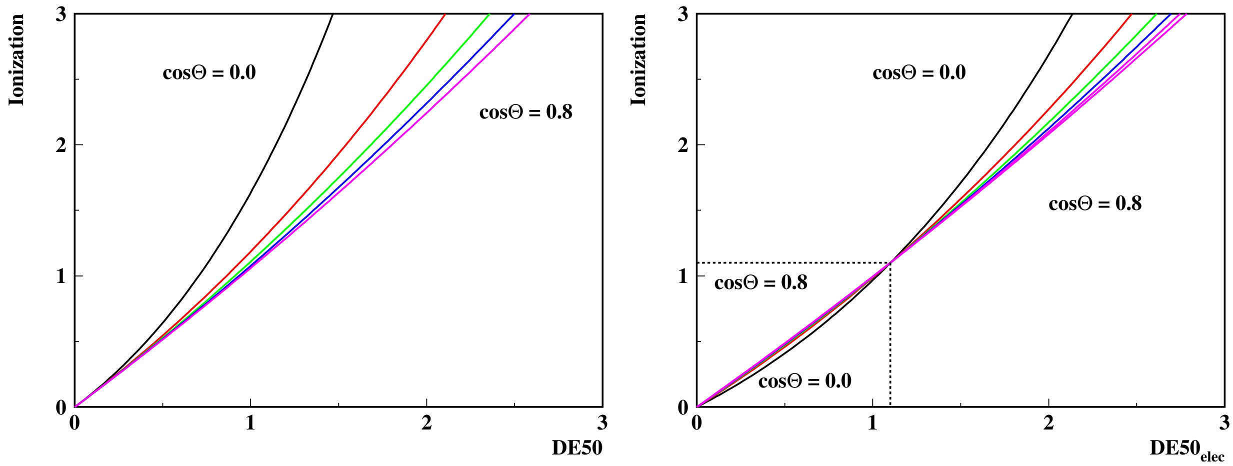

Figure 4: The hypothesized relationship between actual and measured ionization as a function of $\cos\theta$ is shown in plot a. Plot b shows the relationship bewteen I and $\mathrm{DE50}_{\mathrm{elec}}$ as a function of $\cos\theta$. There are 5 curves which correspond to $\cos\theta = 0.0, 0.2, 0.4, 0.6, 0.8$ (black,red,green,blue,magenta).

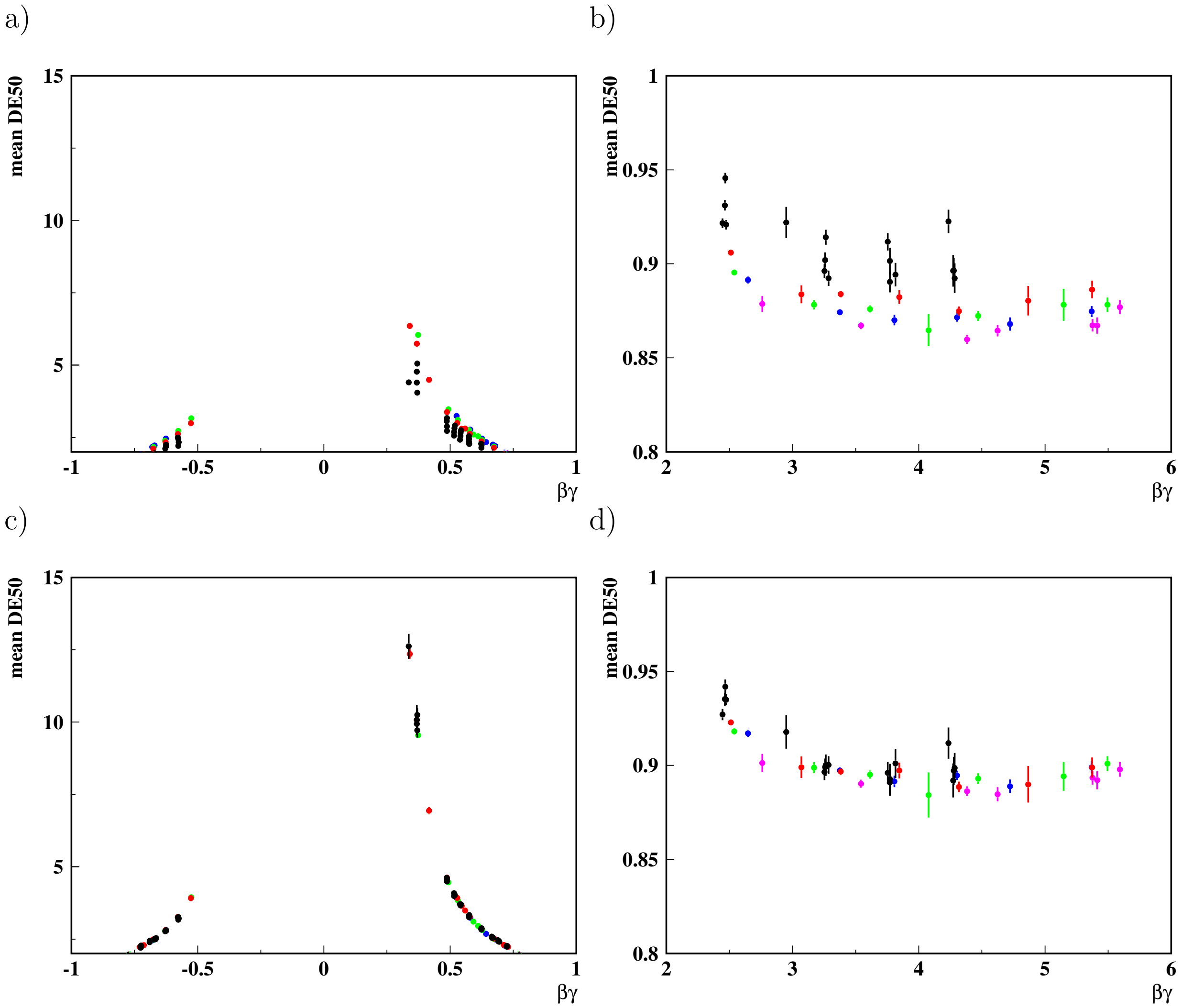

Figure 5: The $\cos\theta$ dependence of mean $\mathrm{DE50_{elec}}$ is shown in plots a & b protons and pions around minimum ionization, respectively. Plots c & d show the mean value of I for the same tracks. There are 5 colors which correspond to $\cos\theta = 0.0, 0.2, 0.4, 0.6, 0.8$ (black,red,green,blue,magenta).

a) b)

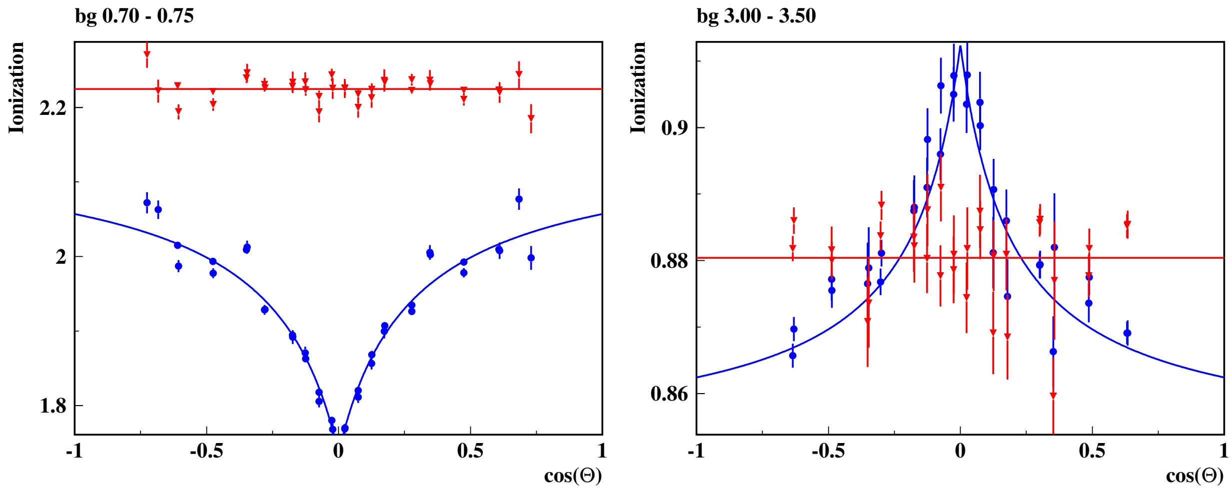

Figure 6: The $\cos\theta$ dependence of mean $\mathrm{DE50}_{\mathrm{elec}}$ (blue) and I (red) after the saturation correction. Plot a shows protons in the "$1/\beta^2$" region and plot b shows pions around minimum ionization.

a) b)

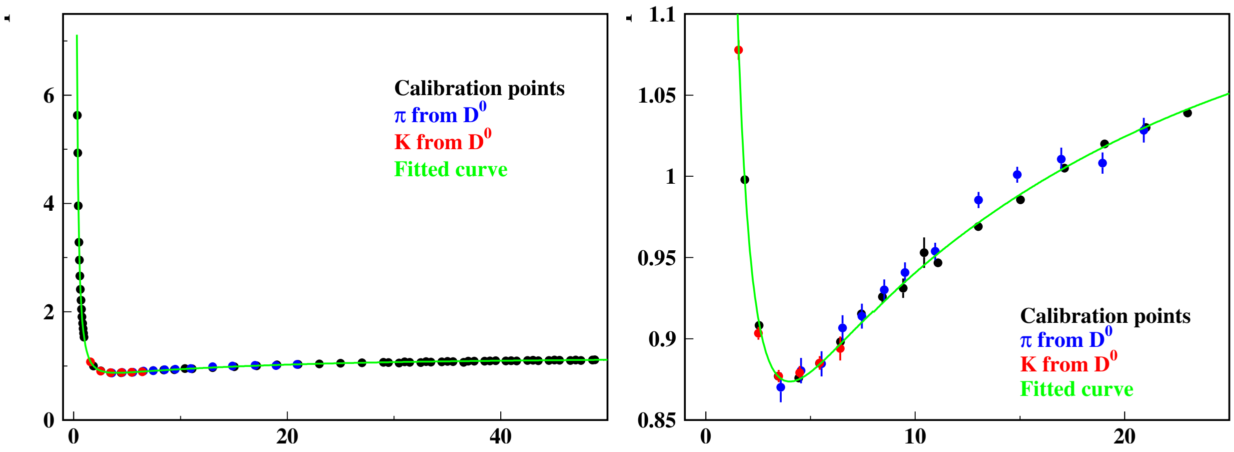

Figure 7: Power Law + 3rd Order Polynomial fit to mean value of I as a function of $\beta\gamma$. The black points are from the proton/μ/π calibration samples. Blue and red points are pions and kaons from D^o decay, respectively. Fit parameters are given in table 2.

a) b)

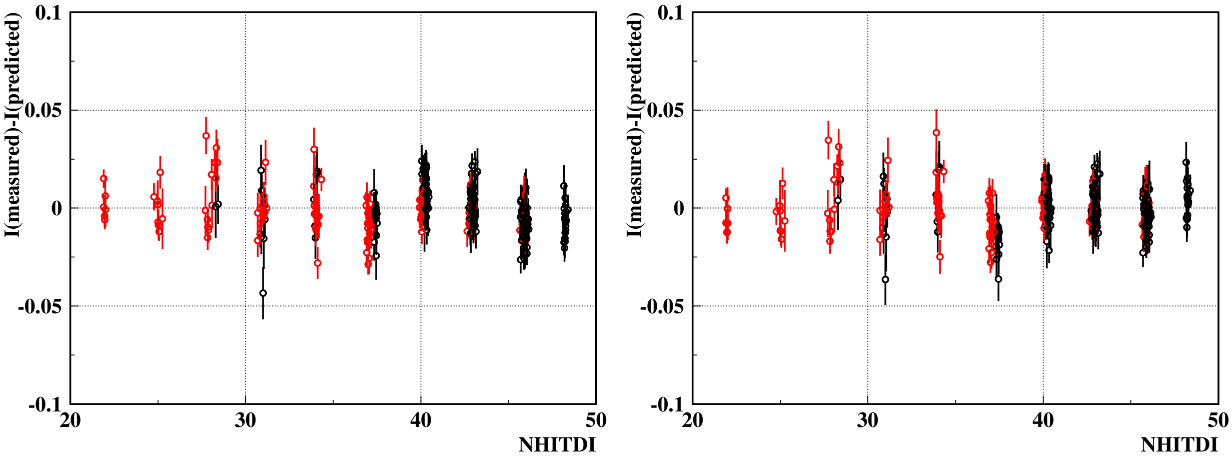

Figure 8: A small but significant running of I with NHITDI is observed in the calibration data. Plot a shows the difference between the value of $\overline{I}$ and mean I as a function of NHITDI. Plot b shows the same points after the correction. Red points are endcap tracks $|\cos\theta| > 0.7$ and black points are barrel tracks.

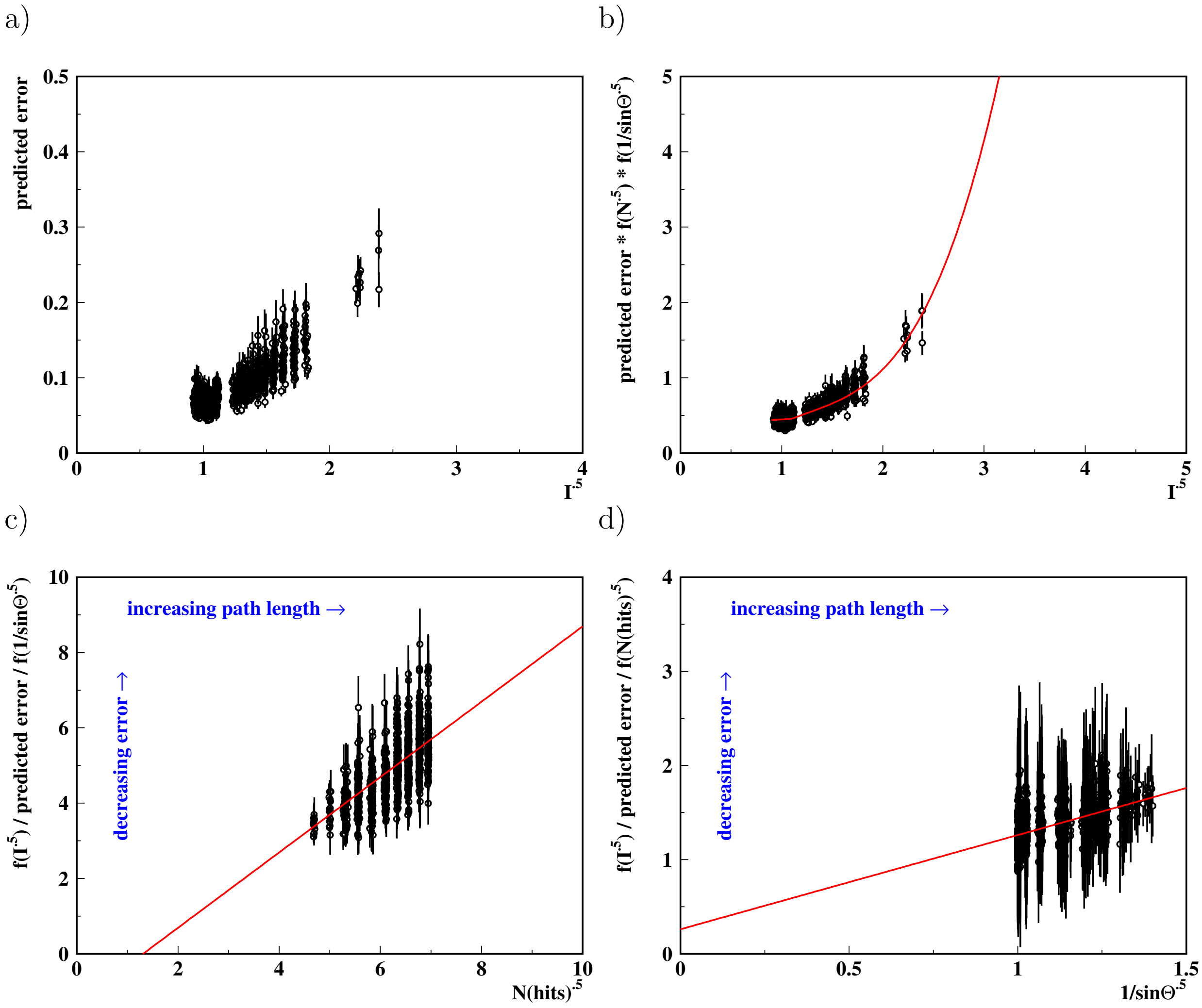

Figure 9: The dependence of σ_I on $I^{1/2}$, NHITDI$^{1/2}$ and $1/\sin\theta^{1/2}$. Plot a is the measured widths of the distributions plotted versus $I^{1/2}$. The next three plots show the dependence on one of the variables after the other two have been removed.

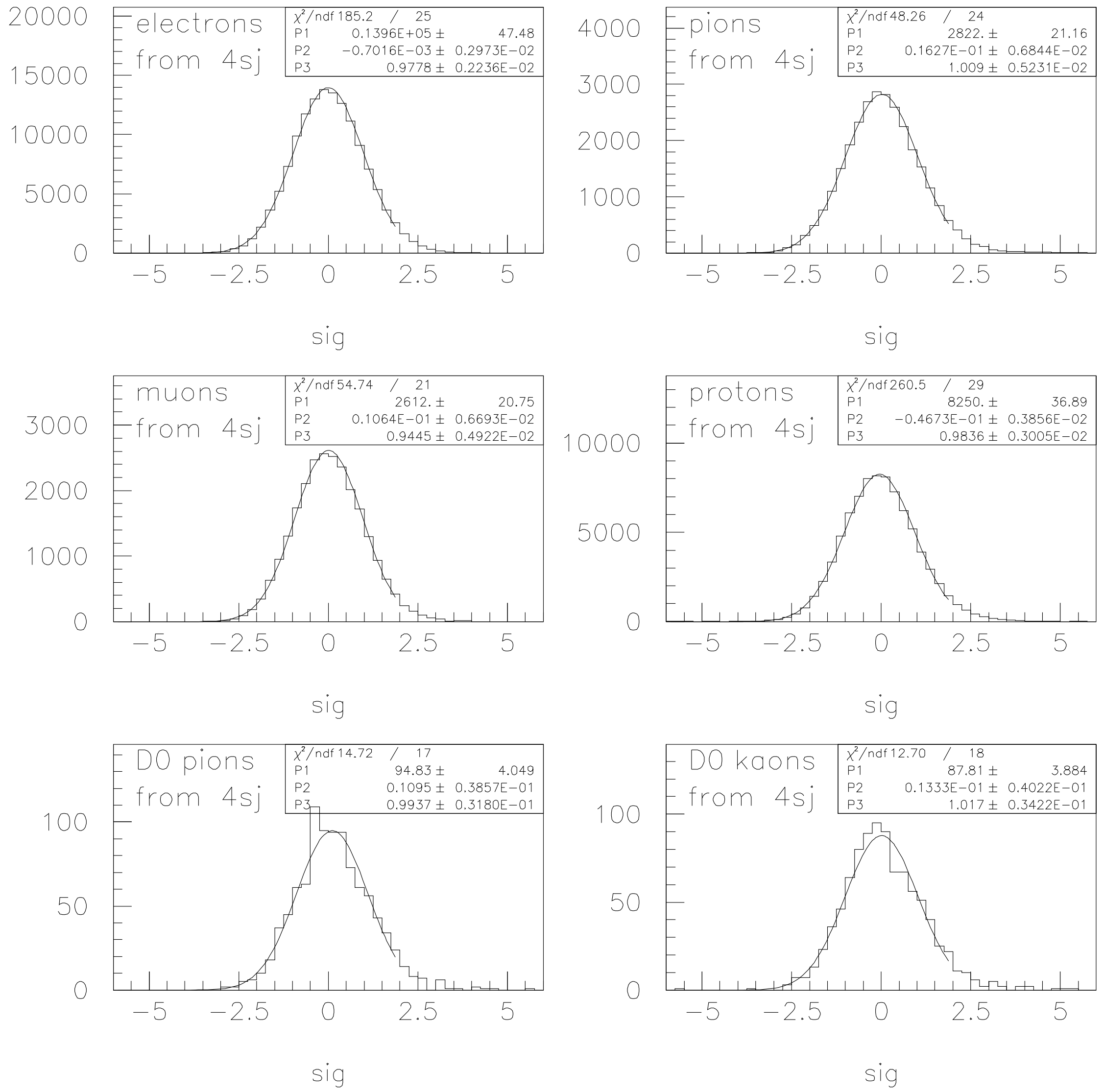

Figure 10: Sigmas for the various particle samples in the 4sJ data set.

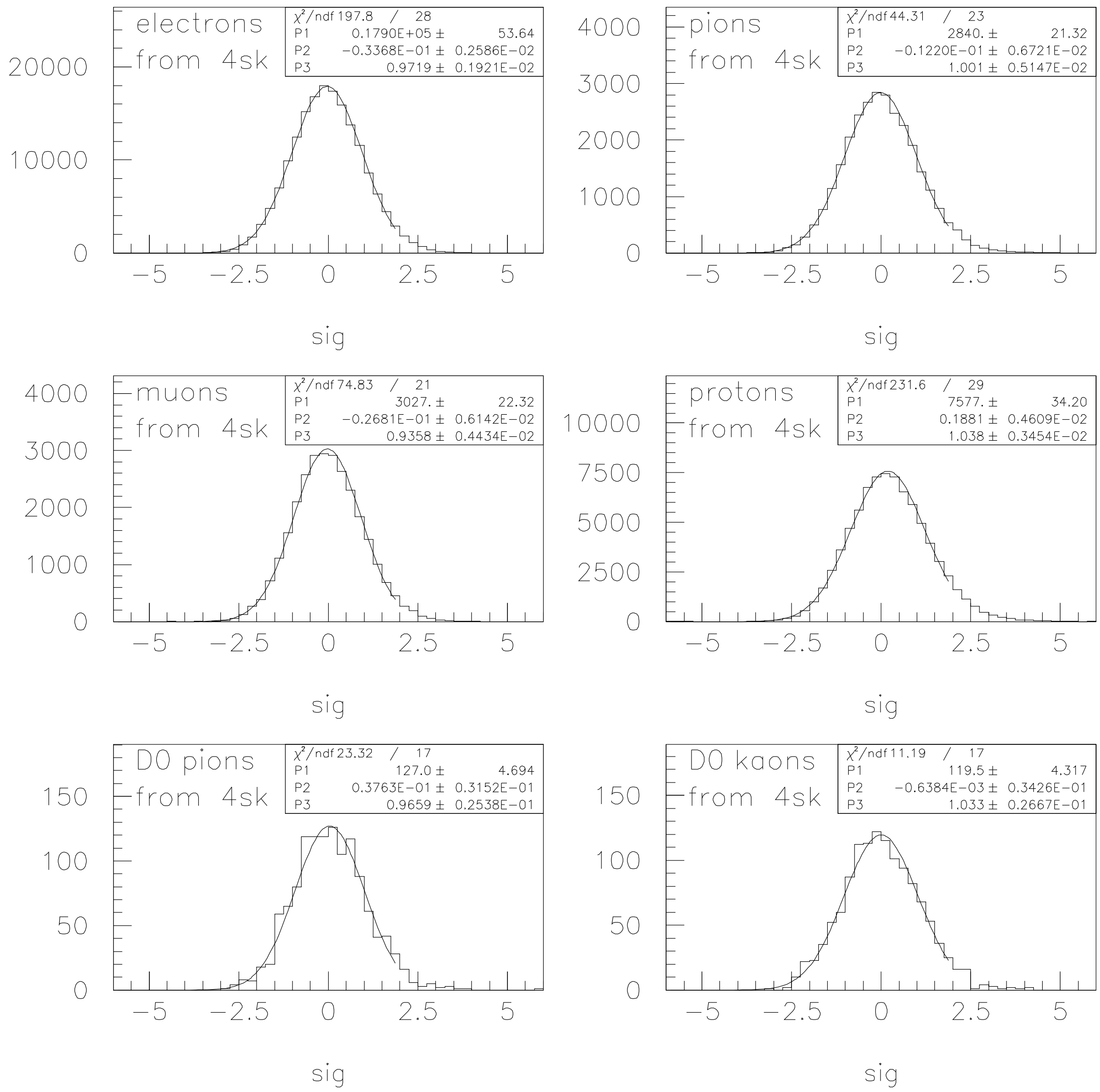

Figure 11: Sigmas for the various particle samples in the 4sK data set.

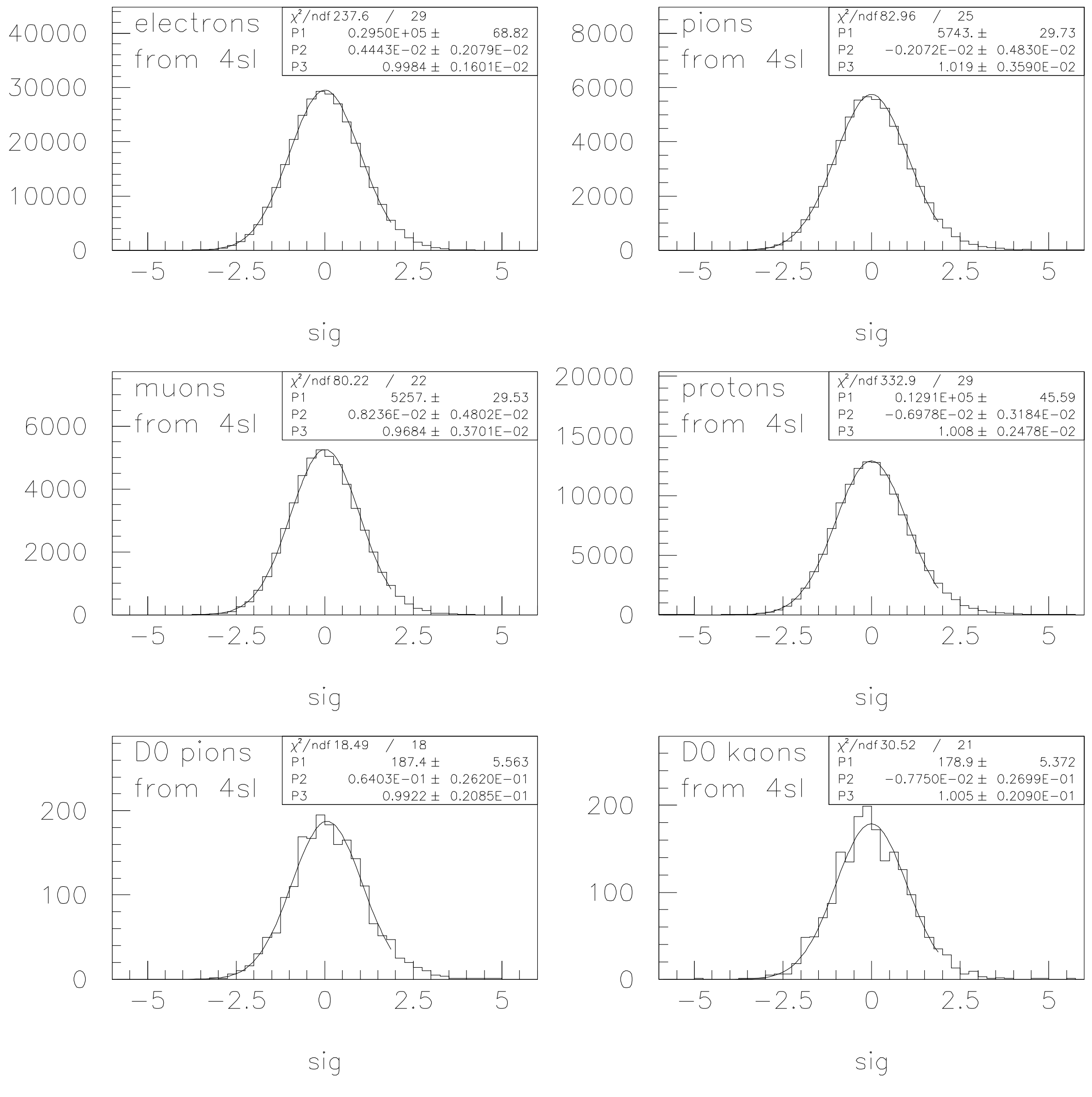

Figure 12: Sigmas for the various particle samples in the 4sL data set.

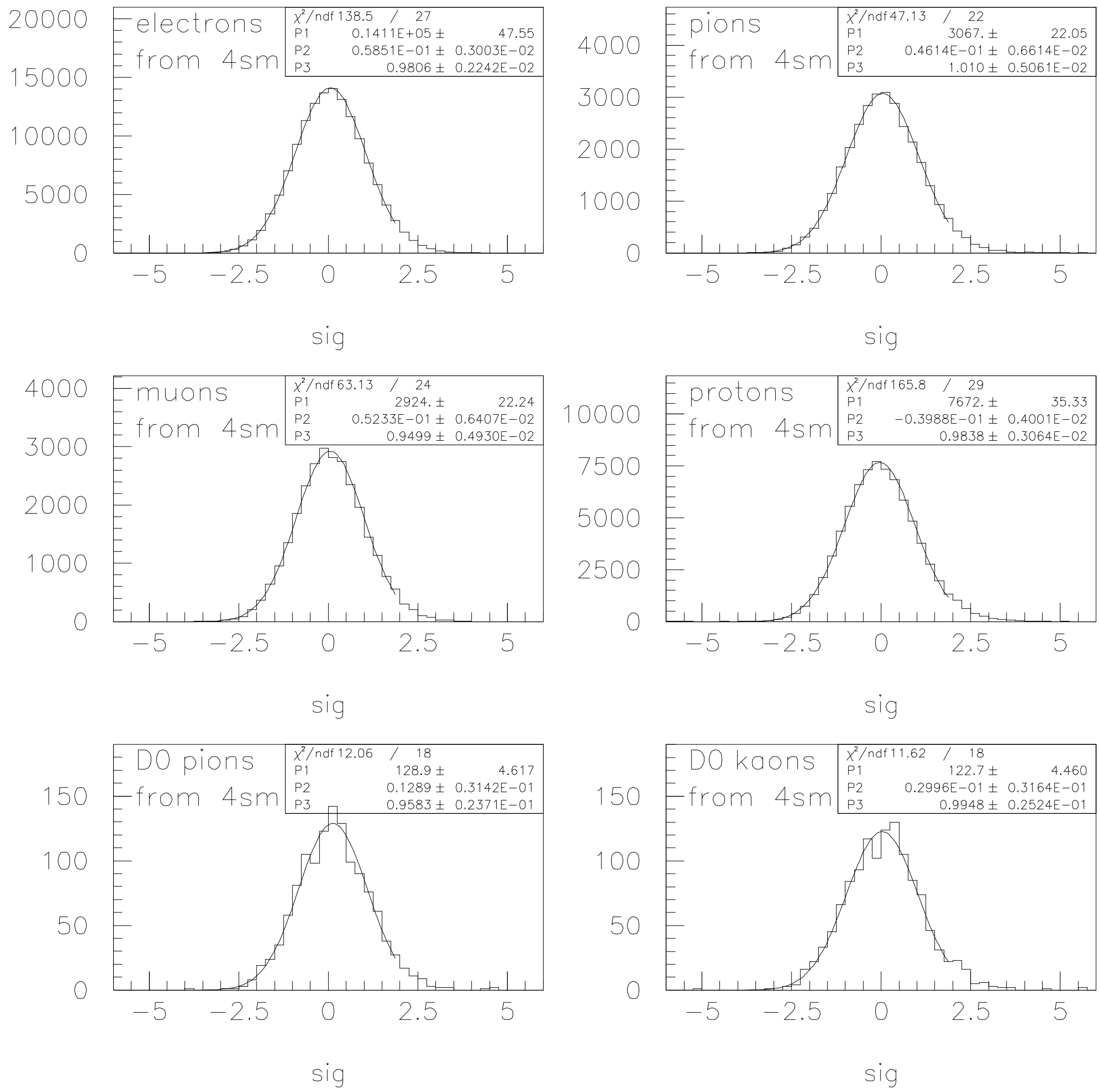

Figure 13: Sigmas for the various particle samples in the 4sM data set.

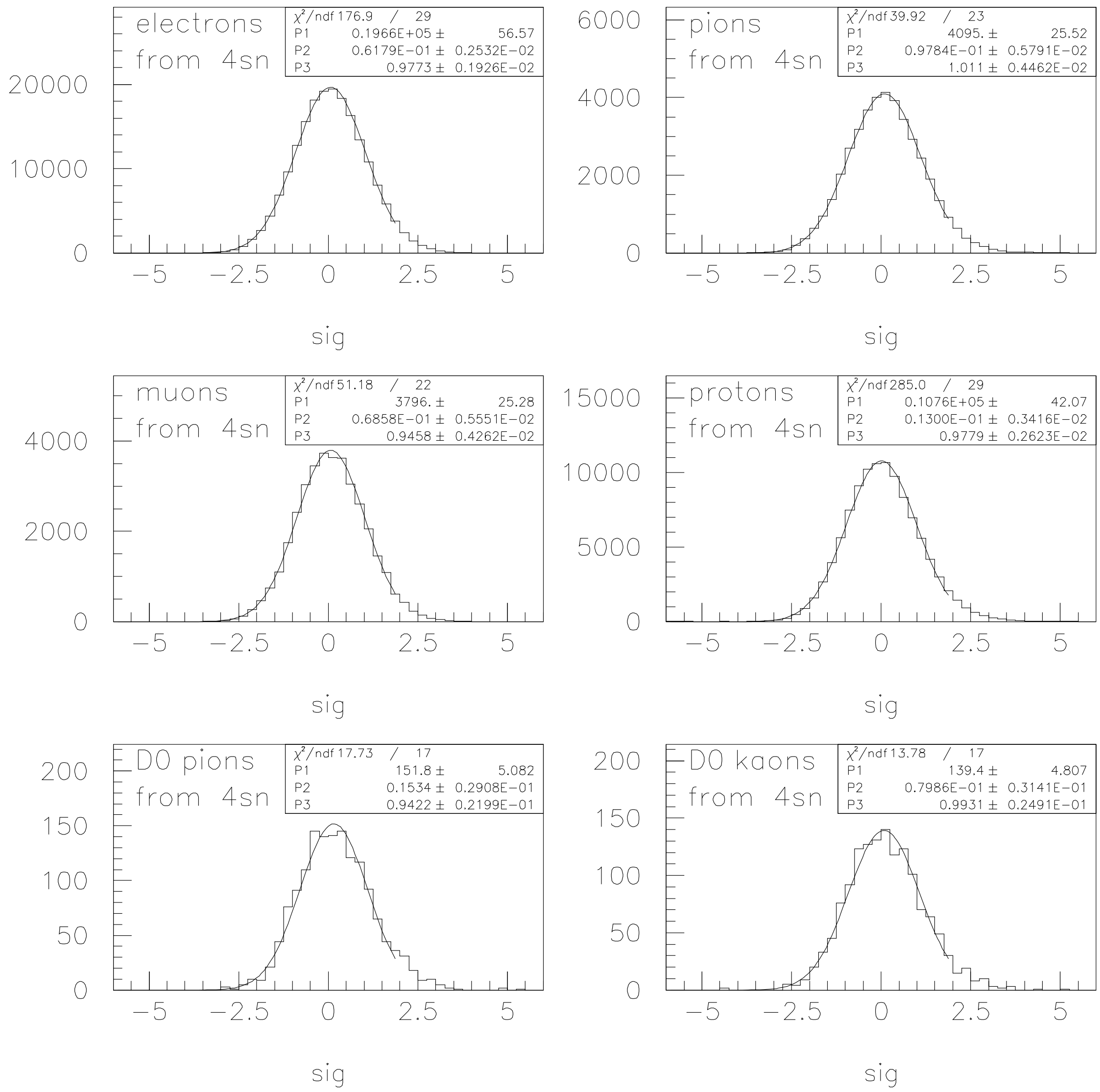

Figure 14: Sigmas for the various particle samples in the 4sN data set.

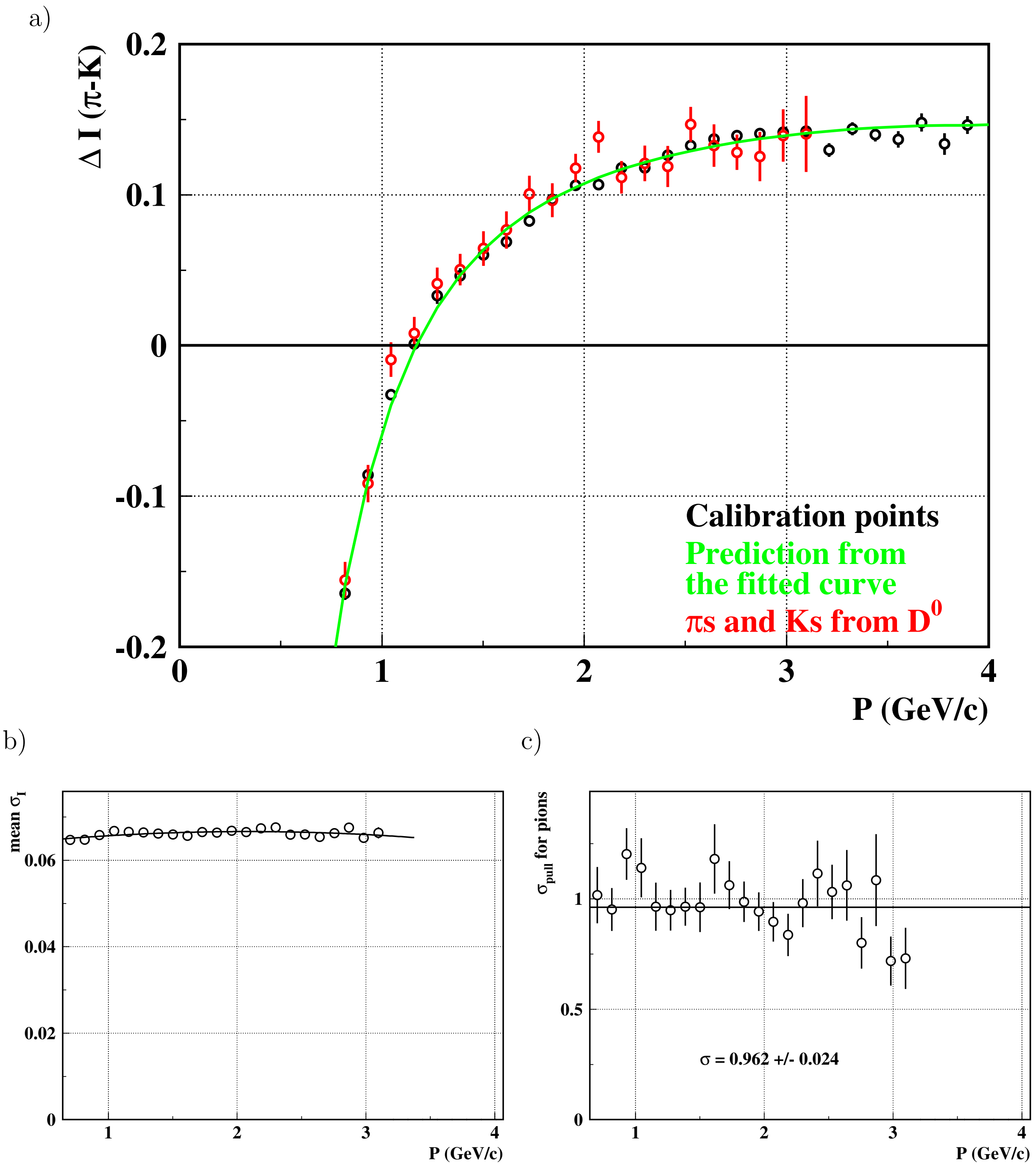

Figure 15: The calculation of K/π separation. Plot a shows the expected difference in mean I for the calibration points (black) and an actual sample of kaons and pions (red). Plot b is the predicted width of the I distribution for a sample of real pions. Plot c is the width of the SGPIDI distribution for those tracks.

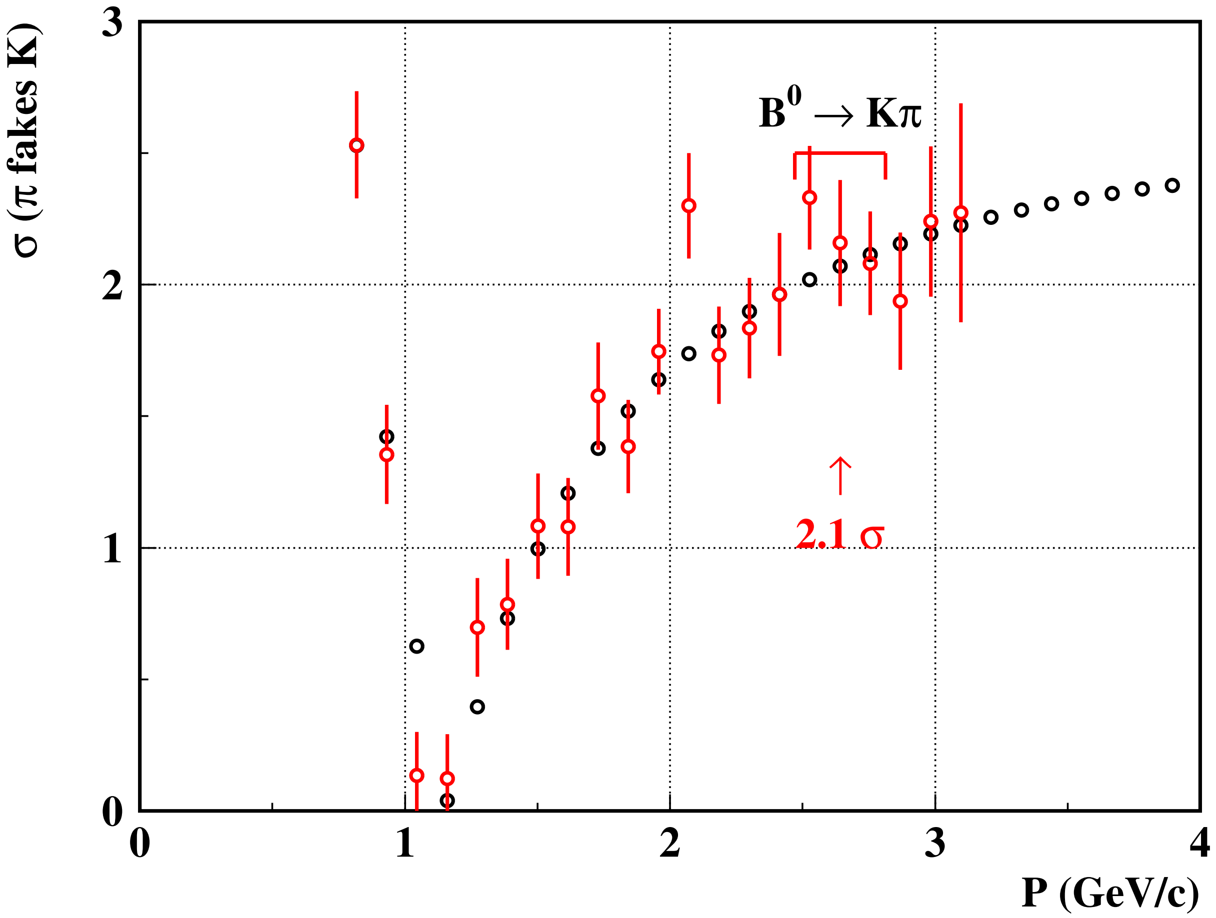

Figure 16: The plot shows the expected K/π separation as a function of momentum.